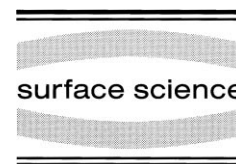




ELSEVIER

Surface Science 448 (2000) 164–178



www.elsevier.nl/locate/susc

# X-ray emission spectroscopy of NO adsorbates on Ru(001)

M. Stichler <sup>a</sup>, C. Keller <sup>a</sup>, C. Heske <sup>b</sup>, M. Stauer <sup>c</sup>, U. Birkenheuer <sup>c</sup>, N. Rösch <sup>c</sup>,  
W. Wurth <sup>a</sup>, D. Menzel <sup>a,\*</sup>

<sup>a</sup> Physik-Department E20, Technische Universität München, 85747 Garching, Germany

<sup>b</sup> Advanced Light Source, E.O. Lawrence Berkeley National Laboratory, University of California, Berkeley, CA 94720, USA

<sup>c</sup> Institut für Physikalische und Theoretische Chemie, Technische Universität München, 85747 Garching, Germany

Received 29 June 1999; accepted for publication 09 December 1999

## Abstract

We report X-ray emission spectra (XES) of the NO adsorbate species on the close-packed Ru(001) surface, and discuss the basis of their interpretation. On this surface NO can exist in two distinct, very different states which coexist in the pure saturated layer and which can be prepared separately by coadsorption with selected superstructures of O atoms. We report symmetry-resolved XES data for these states, and extract atom-specific 2p contributions of adsorbate orbitals which are derived from the molecular 3 $\sigma$ , 4 $\sigma$ , 5 $\sigma$ , 1 $\pi$ , 2 $\pi$ , and 6 $\sigma$  orbitals at the O and N atoms. Their interpretation is facilitated by comparison with very recent density functional calculations [Stauer et al., J. Chem. Phys. 111 (1999) 4704] which use the frozen ground state approximation for the interpretation of the XES data. A consistent picture of the NO–Ru surface bond results which is mainly based on the allyl model, containing charge donation from the adsorbate to the substrate via mixing of the molecular 4 $\sigma$  and 5 $\sigma$  orbitals, and backdonation in the  $\pi$  channels by forming a bonding 1 $\pi$  orbital and a ‘lone pair’  $\pi$ -type orbital on the oxygen often (somewhat misleadingly) denoted as 2 $\pi$  orbital. Finally we discuss some questions of principle for XES of adsorbates, such as the nature of the core-excited state effective in XES of chemisorbates, the influences of relaxation and screening which are neglected in frozen orbital calculations, and possible differences between the valence hole states observed in ultra-violet photoelectron spectroscopy, and in XES at different atoms. © 2000 Elsevier Science B.V. All rights reserved.

**Keywords:** Chemisorption; Low index single crystal surface; Nitrogen oxides; Photon emission; Ruthenium; X-ray emission

## 1. Introduction

X-ray emission spectroscopy (XES) has recently been shown to be a very promising tool for the investigation of the chemical bond of adsorbates to surfaces [1]. An extensively used spectroscopic technique in molecular and solid state studies, XES has been difficult to apply to adsorbates on surfaces due to the very low X-ray

yield for low- $Z$  elements, for which typically 99.9% of core-excited states decay by Auger processes; therefore application to adsorbate studies had a late start [3]. The advent of third generation synchrotron radiation sources with high brightness, and advances in instrumentation, made it possible to utilize the advantages of XES for adsorbate studies as well, and a number of studies have meanwhile been published by the Uppsala group [4–9]. While the final states reached after fluorescence decay of the core hole state are expected to be energetically equivalent to the valence electronic states reached in photoemission,

\* Corresponding author. Fax: +49-89-28912338.

E-mail address: menzel@e20.physik.tu-muenchen.de (D. Menzel)

XES features the advantage that the intensity distribution is highly atom specific due to the localization of the core hole excited in the primary step of the emission process. As the transition matrix element involved is the dipole matrix element, angle-dependent measurements on oriented adsorbates allow the use of symmetry selection rules to assign the spectral features. On the basis of comparisons with model calculations it has been suggested that the observed intensities can be interpreted in terms of the symmetry-resolved local valence electron density of the adsorbates in the *ground* state [1,4–10], at least for the systems studied so far. This means that, contrary to expectation, relaxation effects both in the initial core hole state and the final valence hole state would play a minor role only.

The goal of our study was to test the sensitivity of this technique and its appropriate interpretation by applying it to a system in which clearly different states of the same adsorbate exist. For this we chose the NO species formed in the pure NO layer and by coadsorption with oxygen on a Ru(001) surface. By using these well-known adsorption systems we aimed at getting deeper insight into the differences in bonding of the various molecular adsorbate states which can be observed in this group of systems, and which have been characterized extensively by a large number of methods [11–16]. Adsorption of NO on the bare Ru(001) surface is particularly interesting because two very distinct NO adsorption states (termed  $\nu_1$ -NO and  $\nu_2$ -NO) are populated simultaneously in this case [11,12,15]. These two states can be distinguished for example using vibrational spectroscopy or high resolution X-ray photoelectron spectroscopy (XPS) [11,13,14,17]. Coadsorption of NO with oxygen on the Ru(001) surface under appropriate conditions leads to situations where either  $\nu_1$ -NO or  $\nu_2$ -NO alone is present on the surface [14–17]. Both NO adsorption states have been characterized very thoroughly in the Munich laboratory using different techniques such as vibrational spectroscopy, work function measurements, thermal desorption, XPS [11–17], and accurate geometric structure determination with quantitative LEED (low-energy electron diffraction) [15,16]. These studies showed that  $\nu_1$ -NO sits in threefold

sites, possesses an elongated N—O bond compared to the free molecule and a correspondingly lower vibrational frequency, and carries a large overall negative dipole. On the other hand, the  $\nu_2$ -NO species sits on-top, has a slightly shortened inner bond length, and a positive overall dipole moment of comparable magnitude. This suggests that the two states are distinctly different also in terms of their electronic structure. In fact their characteristics are quite similar to those of electronegative and electropositive transition metal nitrosyl species [15]. Their characteristics are very similar in the pure NO (which is really a coadsorbate layer of the two NO species), and in the O-coadsorbate layers; in fact, the geometries and the vibrational properties are virtually identical in these two different situations. Due to energetic differences in the positions of the respective X-ray absorption resonances at the O 1s threshold (unfortunately not at that of N 1s) the two species can be core-excited separately [17] even when both are present simultaneously on the surface, and can then be compared to the species prepared separately in coadsorption with different oxygen layers. The possibility of their separate preparation in O-coadsorbates allows to study them individually also for N 1s excitation.

Hence XES with resonant excitation should be very well suited to gain more insight into the atom-specific electronic structure of these two different adsorption states of NO. In reverse, the investigation of these well-characterized species should contribute to the understanding and appropriate interpretation of XES of adsorbates. We have therefore carried out an X-ray emission spectroscopic study utilizing an apparatus optimally suited for this purpose. The spectra were generated by fluorescent decay after core excitation into the strong lowest molecular core-to-bound resonance to selectively excite only the target species where possible, and to obtain the highest excitation cross sections possible for N 1s and O 1s excitations of each NO species (see the discussion below as to the initial state of fluorescent decay ensuing from this). Here we describe the experimental techniques and procedures, show the results, and give a qualitative discussion. A theoretical study of the same systems on the basis of ground state electronic

calculations is described in a separate publication [18].

## 2. Experimental

### 2.1. Instrumentation

The experiments were carried out at Beamline 8.0 of the Advanced Light Source at Lawrence Berkeley National Laboratories. This beamline is equipped with a modified spherical grating monochromator with movable entrance and exit slits, with gratings covering the energy region between 100 and 1300 eV. Two refocusing mirrors, one horizontal and one vertical, focus the light to a spot of 50–100  $\mu\text{m}$  on the sample. The end station used at this beamline was constructed at the University of Uppsala and constitutes a high level surface physics apparatus (for a detailed description see Refs. [19–21]). Briefly, it is divided into a preparation and an analyzer chamber. The preparation chamber contains LEED optics, a mass spectrometer and a gas doser system. The analyzer chamber is equipped with a Scienta SES-200 electron spectrometer [22], an X-ray absorption spectroscopy detector [23], and a grazing incidence multiple grating spectrometer [24,25] for the detection of reflected and emitted soft X-ray photons. The sample, which is mounted with its surface close to parallel to the incoming light, can be rotated by the manipulator around the light beam such that any angle between the polarization vector of the synchrotron light and the surface normal can be chosen. Since the analyzer chamber can also be rotated around the axis of the incoming light, it is possible to choose the detection angle independently from the excitation geometry. Thus the angular dependencies of both the excitation and the emission processes can be utilized independently. Some NEXAFS (near-edge X-ray absorption fine structure) data were measured at the SuperESCA end station of ELETTRA in Trieste.

### 2.2. Sample and layer preparation

Following its installation in the ultra-high vacuum (UHV) chamber the sample was cleaned

by Ar sputtering and by cyclical heating between 500 and 1200 K in an oxygen atmosphere of  $5 \times 10^{-7}$  mbar to remove carbon which is close to the surface. To desorb the oxygen the sample was finally heated repeatedly to 1530 K. The cleanness of the surface was tested routinely by high resolution XPS measurements of the Ru  $3d_{5/2}$  peak, the shape of which depends strongly on adsorbate coverage. This makes it possible to detect impurities in the range of some percent of monolayer coverage by their specific surface core level shifts [17,26]. Additional checks by XPS in the energy ranges appropriate for possible contaminants were carried out from time to time.

For the XES measurements of NO the saturated NO layer and two well-characterized coadsorbate layers were prepared. The pure NO layer contains the two NO species in a 2:1 ratio, with a honeycomb arrangement of NO in the hcp and fcc sites ( $v_1$ -NO) surrounding the on-top species ( $v_2$ -NO) [15]. The first coadsorbate layer, labeled  $(2 \times 1)$ -(NO+O), consists of alternating rows of O atoms and NO molecules, all in hcp sites, as shown by the LEED-IV determination [16]. It is produced by adsorbing NO on a  $(2 \times 1)$ -O layer at low temperature (below 150 K). According to the LEED analysis, the N–O bond is stretched, consistent with the vibrational energy, and the simplest interpretation of the observed work function increase is that it is an electronegative species, in analogy to nitrosyls. In most respects (exact geometry; dipole moment; XPS and vibrational spectrum) it is virtually identical to the  $v_1$ -NO species of the pure NO layer; some differences do exist, however, in the parameters measured here which we will describe below. Heating this layer to 440 K desorbs half of the NO and converts the residual layer to a new structure, the  $(2 \times 2)$ -(2O+NO) layer. In this, every second O atom switches from an hcp to an fcc site, and simultaneously the residual NO moves on-top, as shown by quantitative LEED [17]. This coupled desorption–conversion process, which possesses very interesting kinetic aspects, has been investigated in detail before [27]. LEED also shows that now the N–O bond is shorter by 0.10 Å, which is corroborated by the much higher vibrational frequency; measurements of the work function change show

that the top-bound NO possesses a positive dipole. It is virtually identical in most aspects to the  $v_2$ -NO species of the pure NO layer. Quality and homogeneity of these layers were tested by checking their characteristic XPS spectra [11,16,17].

### 2.3. Data accumulation and evaluation

As mentioned, the XES spectra were taken after resonant excitation of an N 1s or O 1s electron, respectively, into the empty part of the  $2\pi^*$ -derived level of the adsorbate, because selection of the optimum energy and incoming angle for maximum coupling to the resonance of the desired species permits to select that species, and considerably enhances the excitation cross-section and therefore the detector signal compared to nonresonant excitation. The bandwidth used for primary excitation as well as for secondary XE was 0.5 eV. The sample temperature during measurements was ca. 80 K. To avoid the effects of degradation of the adsorbate by the intense irradiation, the beam was scanned stepwise over the sample during the measurements by moving the sample; absence of noticeable degradation was periodically checked by comparing the XE spectra and by high resolution XPS. Nevertheless, the initial state of decay which is relevant for the XES spectra is — despite the resonant excitation — the fully relaxed core hole state of the adsorbates, with its energy given by the binding energy (BE) of the adsorbate XPS main line; we will come back to this in Section 4.

The XES spectra shown below were derived from the raw spectra by applying a number of corrections [19–21]. The non-linearity of the energy scale of the two-dimensional detector array of the secondary X-ray monochromator was corrected by a so-called curvature correction. For the calibration of the photon energy scale the elastically scattered photons at the high and the low energy sides of the emission spectra were measured. Between these two peaks the photon energy scale was assumed to be linear. After summation of the energy-corrected single spectra the elastically scattered contribution was subtracted to arrive at the inelastic lines only. For the transformation of the emission spectra from the photon energy scale to

the BE scale of the final states, the spectra were shifted by the corresponding XPS binding energies (see above and discussion) using the following BE values for adsorbed NO (with respect to the Fermi level): 530.3 eV ( $v_1$ -NO) and 531.9 eV ( $v_2$ -NO) for O 1s; 399.9 eV (both species) for N 1s.

Because not only the excitation, but also the decay step of our spectroscopy is governed by the dipole matrix element, the XES spectra can be symmetry-resolved by selection of the fluorescence exit angle; this allows a separation of  $\pi$  and  $\sigma$  contributions of the final states [1,3–9]. Because in both NO species the molecule is adsorbed standing upright on the surface [15,16], only the  $\pi$  contribution is detected in normal emission, while in grazing emission  $\pi$  and  $\sigma$  contributions are measured by the detector. Further data treatment would be easiest if the ratios of the detector efficiency in the energy regions of the O 1s and N 1s spectra for the different angles of measurement, were known accurately which is not the case. Extraction of the  $\sigma$  contribution alone is achieved by subtracting the normal emission spectrum from that at grazing emission. For this subtraction the spectra are scaled (with a factor close to 1) such that underswings are avoided, and flat backgrounds result in the regions where no signal is expected. The sensitivity dependence on the X-ray energy is eliminated by scaling the individual spectra to the sum of the integrals of the spectra measured in the  $\pi$  and  $\sigma$  channels for the respective core hole decay, N 1s or O 1s. This scaling has also been used in the density functional (DF) calculations [18]. The measured spectra then still contain the different fluorescence yields for N 1s and O 1s which are about 1:1.5 [28]. No correction for the latter has been applied to the measured spectra shown because the comparability of the intensity scales of the different spectra is not believed to be that good and because in any case we will make only semi-quantitative arguments for their interpretation.

### 3. Results and interpretation

In Fig. 1 we show the NEXAFS spectra of the pure NO and the two NO coadsorbate layers, for

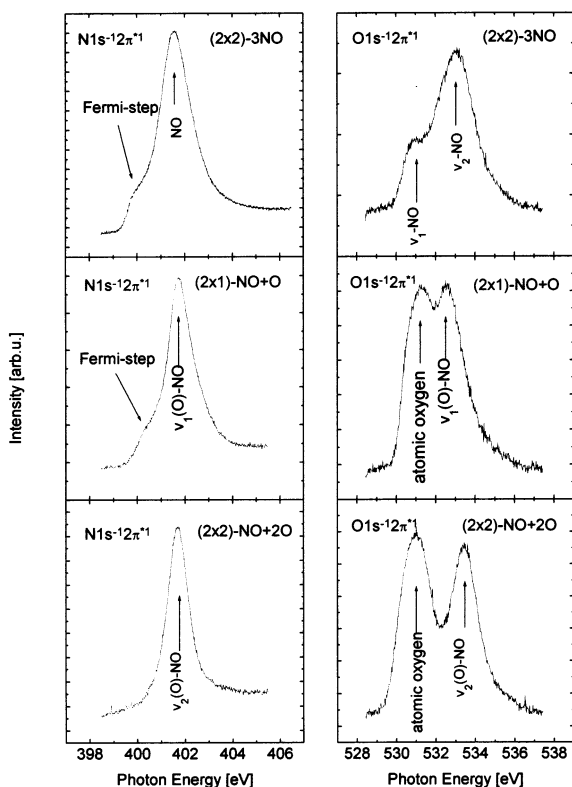


Fig. 1.  $1s \rightarrow 2\pi^*$  photoabsorption (light incident in the surface normal) of various adlayers on a Ru(001) surface at the O 1s (right side) and N 1s edges (left side): pure NO (top),  $(2 \times 1)$ -NO + O (center), and  $(2 \times 2)$ -NO + 2O (bottom).

N 1s and O 1s excitation, measured in the partial yield mode emphasizing the respective N or O Auger yields, with a photon bandwidth better than 0.1 eV. Normal incidence of the incoming photon beam (polarization vector in the surface plane) has been used for optimum coupling to the  $\pi$ -type resonances of the (upright) molecules. For the coadsorbate systems, the O 1s spectra also contain contributions from absorption of atomic O, of course, which however are seen to be well separated energetically. The main function of these spectra here is to demonstrate the selection of the excitation energies used (see arrows); the used bandwidth (0.5 eV for XES; see above) assures the selective excitation of the wanted species only. However, we have to mention that the spectra contain one surprising detail, in that the excitation energies for the assumedly similar species in the

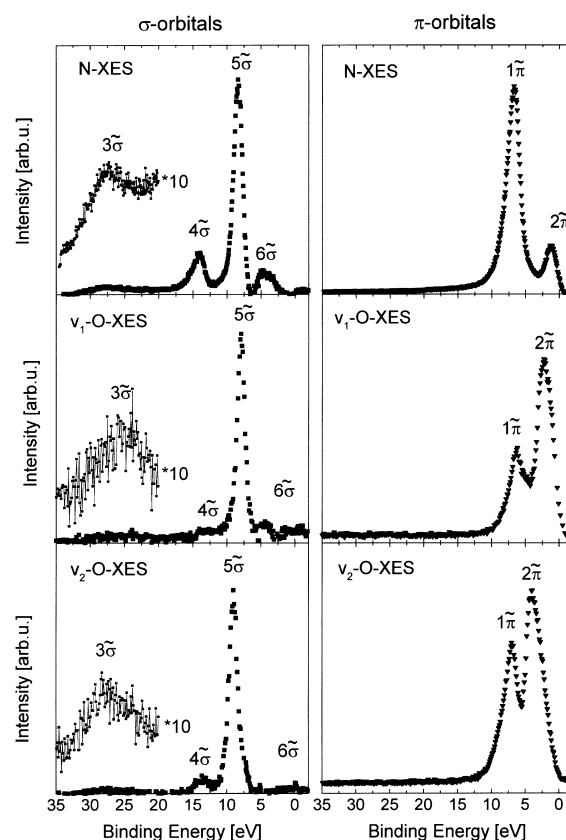


Fig. 2. XE spectra for the pure saturated NO layer on Ru(001) [ $(2 \times 2)$ - $(2 v_1\text{-NO} + v_2\text{-NO})$ ], for N 1s (both species) and O 1s (separate for the two species) excitation, separated in  $\sigma$  (left) and  $\pi$  symmetry (right).

pure NO and the O-coadsorbed situation are not the same for the O 1s excitation, in particular for the  $v_1\text{-NO}$  species. As can be seen from Fig. 1, the O 1s excitation energy for this species is ca. 1.5 eV higher in the coadsorbed layer than in the pure NO layer; the difference for the  $v_2$ -species is smaller (0.4 eV). This is surprising in view of the almost identical geometries and other parameters, including XPS energies (see above). It might be connected to the spread of the resonant orbital (see below), from which different regions may be emphasized under the changing surroundings. Indeed, the NO–NO correlation and distances for the  $v_1$ -species in the coadsorbate (close-packed rows on hcp sites) and in the pure NO layers (hexagons on hcp and fcc sites) are quite different, so this appears pos-

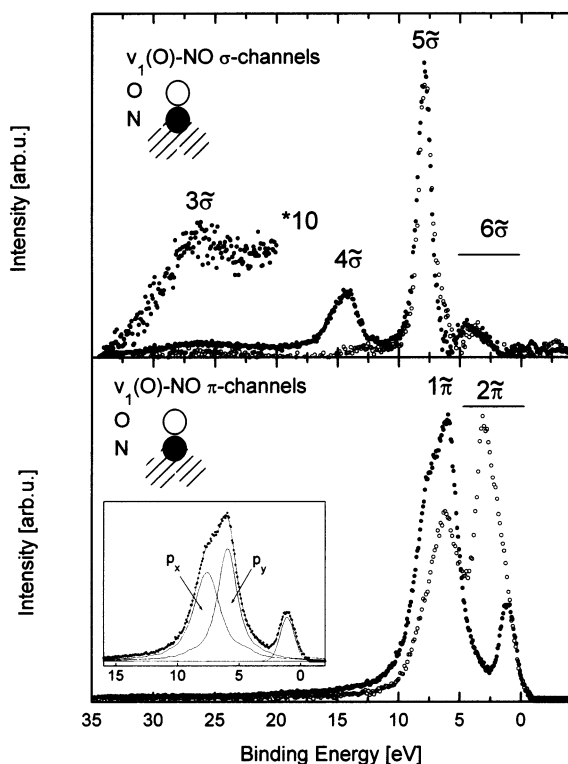


Fig. 3. O 1s (○) and N 1s (●) XE spectra of  $v_1$ -NO in the  $(2 \times 1)$ -NO+O adlayer on a Ru(001) surface, separated in  $\sigma$  (top) and  $\pi$  symmetry (bottom).

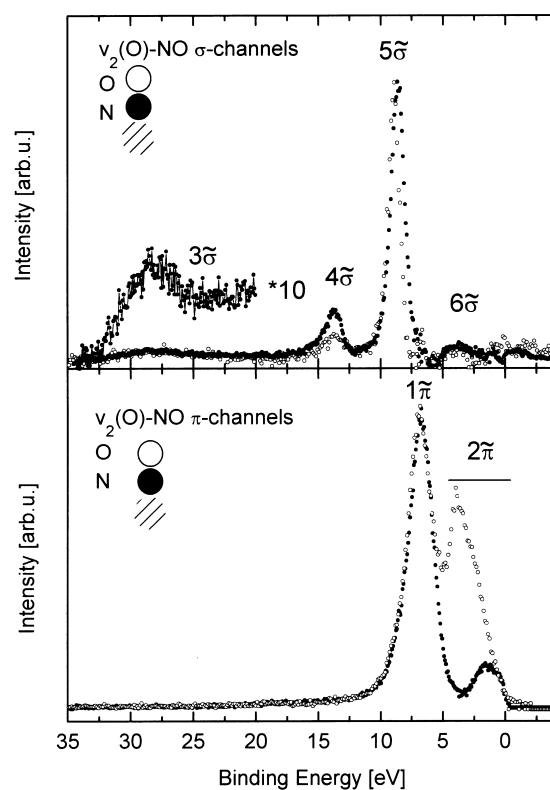


Fig. 4. O 1s (○) and N 1s (●) XE spectra of the  $v_2$ -NO in the  $(2 \times 2)$ -NO+2O adlayer on a Ru(001) surface, separated in  $\sigma$  (top) and  $\pi$  symmetry (bottom).

sible. In fact, the identity of the excitation energies at the N 1s for the very different species is equally surprising. Both findings point at a less than complete understanding of NEXAFS. In view of the identical geometries and vibrational spectra we still believe that the  $v_1$ -species in the two situations are also very similar in their bonding to the surface, even if not in all valence hole spectral features where some differences are also found (see below). We do not discuss the NEXAFS data further but just mention the evidence for a ‘Fermi step’ [23] visible as a shoulder in the N 1s absorption of  $v_1$ -NO.

Figs. 2–4 summarize our XES results obtained in the described way for the pure (mixed) layer, and the separately prepared NO species coadsorbed with oxygen. Comparison of the two sets suggest that the spectra of the pure NO layer can be understood by a weighted sum over the two

separate species in most respects: the O spectra (for which separate excitation of each of the two species is possible; see above) are close to those of the separate species, while the N-spectra are well approximated by weighted sums of those of the two separate species coadsorbed with O, with the  $v_1$  contribution dominating. There are two exceptions to this: the splitting seen in the main  $\pi$  peak for the  $v_1$  species in the coadsorbate system is certainly absent in the pure layer; and the relative intensities of the  $\pi$  peaks of  $v_2$  are different in the two situations (the energies are the same). As we will show below, the first difference is well understandable in terms of the detailed geometry of the respective layers; we have no good explanation for the second one.

Despite these small deviations we believe that this comparison justifies the assumption — derived from the mentioned multitude of other results —

that the main bonding situation for each of the two species in the pure and the coadsorbate situations is essentially the same, as are the molecular geometries, the vibrational energies, and the dipole moments. Comparison to calculations for the separate species [18] is considered as justified, therefore.

Figs. 2–4 then depict the atom-specific XE spectra (resolved into  $\pi$  and  $\sigma$  components as described) of the NO molecules in the  $(2 \times 2)$ -3NO, the  $(2 \times 1)$ -(O+NO), and the  $(2 \times 2)$ -(2O+NO) structures, following excitation of a N 1s or O 1s core electron, respectively, into the  $2\pi^*$  resonance of the NO molecule (and the subsequent relaxation, see Section 4.1). Two aspects in which this spectroscopy is different from valence photoelectron spectroscopy — despite the supposed similarity of the final states — have to be kept in mind when examining these data. The first is the local nature of the decay process which involves the overlap of the corresponding valence level with the core hole concerned. Thus, these spectra yield local, atom-specific valence information [1,3–9]. In Section 4 below, we will address the question whether this atom-specific valence ‘density’<sup>1</sup> is that of the unperturbed ground state or corresponds to the valence electron distribution produced under the polarizing influence of the core hole. The second specific information stems from the fact that in the one-center approximation the dipole matrix element selects, in addition to symmetry, also the angular momentum of the final state [1]. In our case of 1s holes, the partial density projected out by XES is the p density<sup>1</sup>. Due to this angular momentum selection and contrary to ultraviolet photoelectron spectroscopy (UPS) of light adsorbates on d-metals, the XE spectra are not dominated by metal d-density as is the case for UPS, where this makes it difficult to draw any conclusions about adsorbate-induced changes in this spectral region. While this makes the observa-

tion of details in this important region much easier here, it necessarily precludes any information on the metal contributions to the adsorbate bond which are expected to be large for such a d-metal substrate. The p contributions to the surface bond of atoms and molecules of light elements will still be very important and are directly accessible here; some of the changes connected with d (and s) redistribution may be seen indirectly (via orthogonality effects on the p density) but mostly will appear not at all. Thus, our measurements approximately project out the symmetry-resolved, local 2p ‘densities’<sup>1</sup> on the N and O atoms, respectively, separated into  $\pi$  and  $\sigma$  components.

The information we have on symmetry and energy of each peak allows us to assign them and to correlate them with UPS results [29] for all peaks above 5 eV; at lower BE, UPS does not give a clear-cut picture due to the overwhelming emission from metal d-states, as just indicated. Table 1 collects the binding energies of all final states studied according to symmetry and assignment.

In the following we describe the main features seen for the two separate species. A discussion of the most important effects and conclusions is given in Section 4.

### 3.1. $\sigma$ levels

In the  $\sigma$  channel (see upper parts of Figs. 2 and 3) the N as well as the O spectra show a very weak (though definite, see inserts) and broad peak at BE of 28 ( $v_1$ ) and 26 ( $v_2$ ) eV, which we interpret as due to the  $3\tilde{\sigma}$  orbital as final state (as in Ref. [18] we use the orbital labels with a tilde to designate the adsorbate orbitals related to the corresponding orbitals of the free molecule). Its low intensity and large width will be discussed below.

In the BE range from 13 to 14 eV the  $4\tilde{\sigma}$  orbital is expected; the corresponding emission lies at somewhat different energies for the two species. Its considerable intensity is due to the atomic 2p admixture to the corresponding adsorbate orbital. In the isolated NO molecule only oxygen provides a noticeable p contribution to this orbital [18,30]. For our chemisorbed species significant modifications are obvious: for the threefold-bound  $v_1$ -NO

<sup>1</sup>To be sure, the measured XES intensity is given by the square of the corresponding dipole matrix element which contains the respective wave function, not by the density which is the square of the latter. Replacing the former by the latter is an approximation which, however, works well in the semi-quantitative interpretation used here. Therefore it is customary to refer to XES as probing the local (p) density (see Refs [1–9]), even though it really probes the corresponding wavefunctions.

Table 1

XES and UPS binding energies (in eV) of the  $\pi$  and  $\sigma$  one-hole final states with respect to the Fermi level; the XES energies are taken from Figs. 2–4, and the UPS binding energies (angle-integrated measurements) are from Ref. [29] and the subscripts N and O are used to distinguish between signals in the N- and O-edge spectra, respectively

Layer	Edge	$3\sigma$	$4\sigma$	$5\sigma$	$1\pi$	$2\pi_N/2\pi_O$	$6\sigma_N/6\sigma_O$	
$(2 \times 2)$ -3NO	N	27.3	14.0	8.0	6.7	1.1	3–5	XES
	$v_1$ -O	26.1	13.0	7.9	6.3	2.2	3–5	
	$v_2$ -O	27.6	13.6	9.0	6.9	4.0	3–5	
$(2 \times 1)$ -NO+O	N	26.8	14.2	7.8	6.2/7.33	1.1	3–5	XES
	$v_1$ -O	26.2	13.1	7.8	6.2	3.1	3–5	
$(2 \times 2)$ -NO+2O		–	14.2	8.8	5.9	–	–	UPS
	N	28.3	13.7	8.5	6.8	1.4	4	XES
	$v_2$ -O	27.6	13.7	8.9	7.0	3.9	4	
		–	13.9	9.4	7.8	–	–	UPS

as well as for the top-bound  $v_2$ -NO the p character is significantly increased at the N center, whereas, in the case of  $v_1$ -NO (see Fig. 2) the intensity at the O center nearly disappears; for  $v_2$ -NO (see Fig. 2) some intensity remains at the O center.

The most significant chemisorption-induced modification of the electron distribution which is obvious from the combined  $\pi$  and  $\sigma$  channels is the energetic reordering of the  $5\sigma$  and  $1\pi$  levels. While in the isolated molecule the BE sequence is  $3\sigma > 4\sigma > 1\pi > 5\sigma$ , the XES spectra of the chemisorbed species show the sequence  $3\sigma > 4\sigma > 5\sigma > 1\pi$ . It should be noted that the UPS spectra could so far not be interpreted unequivocally in this respect [11,31]; only very recent, angle-resolved data [29] allow a clear assignment. Depending on the adsorbate species we locate the  $5\sigma$  orbital at 7.8 ( $v_1$ ) and 8.5–8.9 ( $v_2$ ) eV in XES.

In the range between 5 and 2.5 eV there is weak  $6\sigma$  intensity at both N and O atoms. Comparison of the  $v_1$ -NO and the  $v_2$ -NO spectra shows that this emission is slightly more pronounced for  $v_1$ -NO than for the  $v_2$ -NO species.

### 3.2. $\pi$ Levels

In the  $\pi$  space (see lower parts of Figs. 3 and 4) the modifications by chemisorption are much more pronounced. Firstly, there is the energetic reordering of  $5\sigma$  and  $1\pi$  orbitals already mentioned. Secondly and more dramatic, new chemisorption-induced states are detected in the region of the Ru d-band, unobservable using UPS. A

direct comparison of XES and UPS measurements is not possible in this region, therefore.

The  $1\pi$  state, which is spatially delocalized over the molecule, lies between 6 and 7 eV for the N and the O atoms of both species. Special attention should be directed at the  $1\pi$  level of  $v_1$ -NO at the N atom in the coadsorbate layer (Fig. 3) which shows a peak at 6.2 eV and a high shoulder at 7.3 eV. We interpret this splitting of the  $1\pi$  orbital as induced by the  $C_s$  symmetry of the  $(2 \times 1)$ - $(O+NO)$  superstructure. This overlayer consists of close-packed rows of O atoms and  $v_1$ -NO molecules, so that the rotational symmetry of the surface is broken and the  $1\pi$  orbitals are no longer degenerate. The  $C_s$  symmetry of the rows leads to the splitting of the  $1\pi$  peak into two strong equally occupied contributions with  $a'$  and  $a''$  character, which can also be viewed as the  $p_x$  and  $p_y$  contributions, parallel and perpendicular to the NO rows (see insert in the lower part of Fig. 3). A comparison of the full widths at half maximum (FWHM) of the fitted curves suggests that  $p_x$  (FWHM 2.7 eV) is aligned parallel and  $p_y$  (FWHM 2.1 eV) perpendicular to the NO rows. Because the NO–NO distances along the rows are smaller than those perpendicular to the rows (2.71 and 4.69 Å, respectively), the electronic interaction parallel to the NO rows is more pronounced and consequently the FWHM is larger. Put in a different way: the stronger coupling along the NO chains leads to a broader one-dimensional band [29] and, since XES sums over the entire band, the overall peak gets broader. Despite the fact that the two NO species

cannot be separated in the N 1s spectra, comparison to Fig. 2 shows clearly that the splitting does not exist in the pure NO layer, as one expects from our interpretation for this layer: the symmetry remains threefold, and the NO–NO distances are increased, because now the NO molecules sit on next-near neighbors. No splitting is resolved at the O atom in either case, but the peak is rather broad there as well.

One of the most striking features of our XES spectra are the  $2\pi_{\text{N}}$  and  $2\pi_{\text{O}}$  ‘lone pair’ orbitals in the range between 0 and 5 eV below the Fermi level, which are inaccessible in the UPS spectra. Both NO species show these features at different energies and strengths at the two atoms: it is much stronger and at higher BE (ca. 4 eV) on the O atom compared to the N atom (BE 1 eV, strength is less than a quarter). The shapes of the peaks at the O center suggest that within a broad level, different energetic ranges are sampled by the O 1s and N 1s holes. The lowest BE component appears to exist on the N end, while at the O atom considerable spectral weight exists at higher BE as well.

## 4. Discussion

### 4.1. XES or RIXS

Before starting the discussion of the details of the experimental results we emphasize why the fluorescent decay after resonant excitation of the core electron in a chemisorbate is aptly treated as *X-ray emission* (XES), thus assuming a decoupled two-step process, and not as *resonant inelastic X-ray scattering* (RIXS) [32], despite the resonant excitation conditions. This is important because only then it is justified to use the XPS energies as the energy content of the initial state of fluorescence decay, that is, the energies of the fully relaxed core hole state in the adsorbate. As stated previously [1,2], this is indicated for strongly coupled chemisorbates, even though the system is excited to the lowest core-to-bound resonance. In an isolated molecular species resonant excitation would, via energy conservation, necessitate to use the

photon energy proper as energy input and, depending on the excitation bandwidth, to use a one-step picture; in that case, the overall process corresponds to RIXS. It has been known for more than a decade [33–36] that for strongly chemisorbed systems on metal surfaces the shapes of Auger decay spectra do not depend on the excitation energy, and in particular that there is no difference between resonant and non-resonant excitation. Thus, the localized core exciton created by resonant dipole-coupled core excitation decays much faster than the core hole. Very recently it has been shown directly that in such systems the probability of survival of a localized core exciton for the entire core hole lifetime is very small indeed [37]: in over 90% of the decay processes, the excited electron in a bound molecular level above the Fermi level will tunnel into the metal taking its energy (and phase) information with it on a time scale much faster than core hole decay. Screening charge flowing back onto the adsorbate at the Fermi level on an even shorter timescale [37,38] neutralizes the molecule again. This sequence of events makes the final state of this process — which is the initial state of fluorescent decay — independent of the path of primary excitation. Therefore the vast majority of the observed fluorescence photons do not contain any information from the resonant excitation, so that our dominating overall process corresponds to XES and not to RIXS, even though we use resonant excitation to tune to the wanted species and maximize the cross section by proper selection of both energy and angle of the photons, utilizing dipole selection rules. We stress that this would *not* be the case for weakly adsorbed species; in physisorbed Ar, for instance, between 20 and 80% (depending on the exact situation) of the resonantly excited electron survives localized up to the time the core hole decays [39,40].

For the discussion of the experimental results we start with the site-specific interpretation of the NO XE spectra, drawing on the DF calculations performed by Staufer et al. [18]. We will implicitly assume that the atom-specific p ‘densities’<sup>1</sup> seen in this spectroscopy can be discussed in terms of ground state one-particle orbitals. This approximation will be discussed subsequently.

## 4.2. Interpretation of the results for chemisorbed NO

### 4.2.1. $\sigma$ Channels

The  $\sigma$  channels of top-bound  $v_2$ -NO and bridge-bound  $v_1$ -NO are dominated by three clearly separated features which have been labeled  $3\tilde{\sigma}$ ,  $4\tilde{\sigma}$ , and  $5\tilde{\sigma}$ . Energetically these peaks are localized below the Ru d-band. In addition there is weak intensity in the region of the Ru-d-band which has been labeled  $6\tilde{\sigma}$  and which is very characteristic for the chemisorbed NO.

We start with the  $3\tilde{\sigma}$  final state. As expected from its large energy separation, and corroborated by our DF calculations [18] this deep final state does not interact with any other orbital and thus entirely retains the character of the  $3\sigma$  level of the isolated NO molecule. The weak intensity can be explained by the dominant (though not exclusive) atomic O 2s character of this molecular orbital, which is not detected in XES. The calculations have shown that there is some p admixture in this orbital. An additional contribution could be caused by deviations from the one-center approximation; it should still be a sharp peak then. Its large width certainly is due to many-body effects well known for inner valence ionization of small molecules: the  $3\tilde{\sigma}$  state is not a good one-electron state but contains admixtures of many higher excitations. Many of the latter may contain p character, contributing further to its visibility in XES.

The  $4\tilde{\sigma}$  p contributions of chemisorbed NO are mostly localized at the N atom. This is in contrast to the isolated NO molecule, where the molecular  $4\sigma$  NO orbital does not exhibit any N p-contribution as already shown by Schichl and Rösch [41] and corroborated by our recent calculations [18]. Hence, the  $4\tilde{\sigma}$  orbital of chemisorbed NO has to be described as a mixture of the  $4\sigma$  and  $5\sigma$  orbitals of the isolated NO molecule as shown schematically in Fig. 5, since only the  $5\sigma$  orbital can contribute p-population at the N atom; metal states are well separated in energy and therefore do not contribute significantly. A detailed analysis of the ratios of the  $4\sigma$  and  $5\sigma$  admixture can be found in Ref. [18]. According to that work, the reduction of the  $4\tilde{\sigma}$  level at the O center can

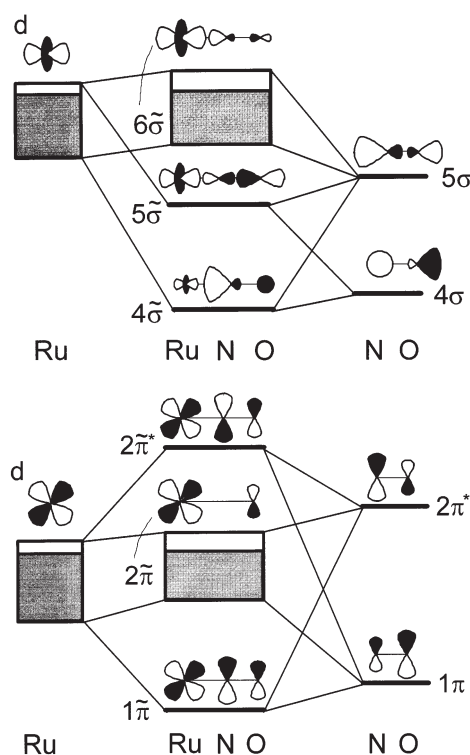


Fig. 5. Schematic representation of the three-orbital interaction of NO with a d-metal surface like that of Ru, shown separately for  $\sigma$  symmetry (top) and  $\pi$  symmetry — the allyl model (bottom). Occupation of the metal d states is indicated by gray shading.

be rationalized by phase arguments. While the  $4\sigma$  and  $5\sigma$  orbital contributions to  $4\tilde{\sigma}$  have the same phase at the N atom, they cancel each other to a large extent at the O atom. This stresses the importance of *wave functions* over *p-densities*<sup>1</sup>. In summary, the chemisorptive interaction with the substrate induces strong rehybridization of the  $4\sigma$  and  $5\sigma$  orbitals in comparison to the isolated NO species.

The most significant difference in the  $\sigma$  channels between bridge bound  $v_1$ -NO and top bound  $v_2$ -NO is the slightly increased  $4\tilde{\sigma}$  intensity at the N center for  $v_1$  compared to  $v_2$ , and the stronger reduction of the O  $4\tilde{\sigma}$  intensity for  $v_1$  compared to  $v_2$ . Staufer et al. [18] explain this by site-specific bond elongation and (marginal) shortening, respectively, of these two NO species. Their different bond lengths yield different shapes of the

molecular orbitals which in turn lead to a different interference or mixture of the  $4\sigma$  and  $5\sigma$  orbitals, resulting in a more perfect cancellation of the  $v_1$ -NO  $4\tilde{\sigma}$  orbital at oxygen and a slightly increased intensity at nitrogen. Both  $4\tilde{\sigma}$  and  $5\tilde{\sigma}$  orbitals exhibit bonding character between the substrate and the NO adsorbate.

In contrast, the  $6\tilde{\sigma}$  final states can be interpreted as anti-bonding linear combinations of proper Ru d orbitals with NO  $\sigma$  orbitals. Interaction with extended metal states leads to the large width of the level and its variable energy localization (see Table 1).

#### 4.2.2. $\pi$ Channels

The introduction of XES into the arsenal of surface science methods, made possible by the third generation of synchrotron light sources, has brought new information on the adsorbate bond, which in turn led to a reappraisal of time-honored models. In particular the traditional frontier orbital model of CO and N<sub>2</sub> bonding to transition metal surfaces, which is usually referred to as Blyholder model [42], has been refined [6,7,41] to a more complex three-center concept usually demonstrated for the allyl radical ('allyl model') [43,44]. The most significant correction thus introduced is the formation of three completely new chemisorbate orbitals — a totally bonding orbital, a kind of 'lone pair' orbital (localized on the metal and on the outer atom), and an anti-bonding orbital by linear combination of the adsorbate  $2p_{x,y}$  orbitals (or, if one starts from the molecule, of its  $1\pi$  and  $2\pi^*$  orbitals) with a suitable set of substrate d orbitals. In Fig. 5 we give a schematic view of the important orbital interactions of this model.

This bonding concept for diatomic molecules on transition metal surfaces is basically confirmed for the NO chemisorption on Ru by our experimental XE spectra presented in this paper. The  $1\tilde{\pi}$  level is identified as the totally bonding mixed orbital, which is mainly composed of the bonding molecular  $1\pi$  orbital with only minor contributions of metal orbitals and of the anti-bonding  $2\pi^*$  orbital. In contrast, the  $2\tilde{\pi}$  feature, which is identified as a set of 'lone pair' orbitals, is dominated by substrate contributions. Only the small admix-

tures to these states which are localized at the adsorbate cores are detected by the XE process. The energetic shift of the  $2\tilde{\pi}$  between the N and O spectra can be rationalized by stemming from different samplings of the metal manifold, implying that at the high-energy end of this manifold the adsorbate contribution is predominantly localized on the O center, while at the low-energy end some contributions at the N atom also exist. In accordance with the allyl model these 'lone pair' orbitals produce larger wave function amplitudes at oxygen and much lower amplitudes at nitrogen. The DF calculations [18] show that these orbitals still possess bonding character between the substrate and the nitrogen atom. The doubly anti-bonding  $2\tilde{\pi}$  orbital of the allyl model is unoccupied and can therefore not be observed by XES, but the  $\pi^*$  resonance seen with NEXAFS (Fig. 1) derives from it. The influence of symmetry and surroundings on the NEXAFS energy of  $v_1$ -NO (see above) may derive from the manifold of states contributing to it.

A comparison of the XE spectra of the 'electronegative'  $v_1$ -NO and the 'electropositive'  $v_2$ -NO species indicates the electronic differences in the  $\pi$ -system. Firstly, the  $1\tilde{\pi}$  and  $2\tilde{\pi}$  binding energies of  $v_2$ -NO are higher in comparison to the  $v_1$ -NO energies. Because of the symmetry-induced splitting of the  $1\tilde{\pi}_N$  orbital of  $v_1$ -NO in the coadsorbate layer, this statement must be applied to the center of gravity of this peak. Secondly, the ratio of relative intensities of  $1\tilde{\pi}$  and  $2\tilde{\pi}$  signals at the O atom is different for  $v_1$ - and  $v_2$ -NO. While for  $v_1$ -NO the  $2\tilde{\pi}$  peak is more intense in comparison to  $1\tilde{\pi}$ , the situation is opposite for  $v_2$  (this conclusion is somewhat weakened by the difference in the  $v_2$  spectra for the pure NO and the O-coadsorbate case). Thus, backdonation from the metal to the adsorbate is more pronounced for  $v_1$ -NO. This leads to a weakening of the intramolecular bond of the latter, in agreement with structural and vibrational data. This analysis also rationalizes why the simpler argument of changes in  $\pi$  backdonation as basis of the different character of the two species, as put forward earlier [15], works quite well. Overall, the differences between the two types of adsorbates are seen to be not very pronounced.

### 4.3. Two critical aspects

#### 4.3.1. Ground state approximation versus relaxation

In this section we address two crucial questions which concern the interpretation of intensities and energies of XES, respectively. As to the relative intensities within a spectrum, Nilsson [1,2] has discussed this topic in detail. He argued that, based on the so-called *final state rule* for simple metals [45,46], these should be governed by the final state configuration, that is, the valence hole state; influences of the initial state, that is, of the core hole, should be small. In a next step the valence hole state is then represented by the ground state wave functions. In all previous computational work [1–9], as well as in our treatment [18], this approximation has been shown to work very well, that is, calculated spectra reproduce the measured ones to good approximation. Partially taking relaxation phenomena into account led to poorer agreement.

In the two-step picture justified in Section 4.1, XES of an adsorbate consists of a transition from the adsorbate core hole state (fully charge transfer-screened, see Section 4.1) to the equally fully relaxed valence hole state. It is well known that even in simple molecules considerable charge redistribution occurs as a reaction to core, but also to valence, ionization. This not only has a distinct influence on the measured energies (expressed by relaxation shifts), but also on the wave functions and charge distribution, which in the ionized species can be very different from the ground state. On the other hand, the ground state approximation described above assumes that the relative intensities of the XES peaks can be used directly to deduce at least semi-quantitatively the p ‘density’<sup>1</sup> at the respective core hole location as it exists in the ground state situation. Only by this assumption has it been possible to draw conclusions about the orbital charge distributions in previous and this work on adsorbate XES. The justification is heuristic: the intensity distributions and the energetic ordering derived from this assumption are in very satisfactory agreement with the experimental results; all decay channels can be reproduced; and the ratios of the relative intensities agree quite well between experiment and calcula-

tion. Thus this analysis leads to a consistent picture of the surface bond. In the present work we arrive at the same conclusion. As laid out in detail in Ref. [18], the intensity distributions in calculation and experiment agree well. On the other hand, agreement was poorer [10] when a physically more appropriate initial state was used, that is, when the calculations were based on a relaxed core hole state, essentially following the initial state rule. This finding supports the use of the ground state approximation; therefore, we have used it here as well, and we believe that the main conclusions about the bonding mechanisms, in particular the importance of orbital mixing induced by chemisorption, are reproduced correctly.

However, one cannot deny that the real process must be quite different. Charge redistribution relative to the ground state as a reaction to ionization, both by charge transfer screening from the substrate to the adsorbate and by charge redistribution on the adsorbate, *must* be extensive. One might in fact have expected that this would make a simple analysis of the spectra very difficult, contrary to the conclusion just given. It appears very important, therefore, to try to understand *why* such a simple and obviously incorrect model seems to work so well. For one, charge relaxation and redistribution processes occur in both the initial and final states of XES and their effects can therefore partly cancel. Thus, any treatment which would consider relaxation processes only in *one* of the states, initial *or* final, should indeed be worse than the ground state approximation. However, while such cancellation might work quite well for the *energies* to be discussed below, the wave functions and their overlap, and with them the *intensities*, should be influenced quite strongly: the polarization of a certain orbital by a localized core hole, compared to that by a distributed valence hole, should be quite different and may, in extreme cases, go in the opposite direction. Furthermore, since we probe the density or rather the wave functions<sup>1</sup> very locally, via its overlap with the core hole (one of the main virtues of the XES method), consequences should be felt. For instance, when we argue about the localization of certain orbitals on one or the other atom, the different polarization effects by a localized or an

extended hole should become noticeable, but within the accuracy of our analysis this is not the case.

We must admit, then, that at present we cannot answer the important question why such a simplified interpretation works so well, and does better than first attempts at more sophisticated treatments [10,47,48]. Further theoretical work is necessary to analyze the situation and find an explanation. Meanwhile we hold use of the ground state approximation as justified in a heuristic manner; a critical attitude towards the conclusions is indicated.

#### 4.3.2. Inequality of XES and UPS energies

The second critical aspect concerns the energies. For these, the agreement between measured values and those calculated on the basis of the ground state model is by far less satisfactory than for the intensities, as noted in Ref. [18]. In the ground state approximation, the orbital energies calculated with a DF method are compared with the measured ionization energies. This simple approach is known to have no solid theoretical basis for the commonly used exchange-correlation approximations [49,50] and sometimes yields poor results. A direct calculation of ionization energies for models comparable in sophistication to those used for the ground state treatments (large clusters or slabs) is still lacking and therefore a well founded comparison is not feasible at present. However, there are two obvious points in the experimental energies (Table 1) that warrant discussion. One concerns the comparison between XES energies for the nominally *same* final state reached via *different* core excitations, and the other the comparison between those and the corresponding UPS energies.

Usually it is asserted that the valence hole states reached in XES are the same as those obtained in UPS [1–3]. This implies that in both cases the final states are the respective lowest valence hole states of the system; it would mean furthermore that the XES energies measured for the same final state via two different core holes should also be the same. Obviously this is not the case for all orbitals (see the compilation in Table 1). A possible explanation offered above in the case of the  $2\pi$

manifold was that broad distributions of mixed orbitals result from the chemisorptive interaction, from which projection on the local p density<sup>1</sup> of states afforded by XES picks different energy ranges depending on the core hole location. In other words, there is a whole manifold of ‘lone pair-type’ final valence hole states; different members of this manifold are reached from different initial core hole states. If this is so, then the equality of final states breaks down and the final states seen in the different spectra can be different. Then one would also not expect any necessary equality to UPS energies. After very long time the final states may be the same for all of these processes (implying relaxation processes *following* the spectroscopic event) and be stationary states of the system, but the measured probe particle (XES photon or UPS electron) can still carry information on a state that has been determined by dipole selection and is only partially relaxed. This could explain both the differences between XES at different atoms, and between those and UPS energies. Further differences will come from the band dispersion observable in UPS; XES should see a weighted average over those states because of the poorly defined momentum of the final state, so comparison should be made to the center of gravity of the (angle-resolved) UP spectra. To approximate this situation, we have compared to angle-integrated measurements in Table 1. Finally, there could be a contribution from the nuclear evolution of the adsorbate atoms during the core hole lifetime. In any case, it appears that one cannot generally expect that XES energies should be equal on different atoms, and should further be equal to UPS energies. Thus, one has to be very careful with any argument based on them that attempts to go beyond a qualitative statement.

## 5. Summary

We have presented experimental XES of the two basically different NO species which can be prepared on Ru(001), together or separately (by the use of coadsorption with atomic oxygen). The spectra were recorded at Beamline 8.0 at the

Advanced Light Source in Berkeley with the XES endstation developed at Uppsala University. After resonant excitation of O 1s and N 1s core electrons it was possible to observe six different fluorescence decay channels for both NO adsorbates, which can be correlated with the  $3\tilde{\sigma}$ ,  $4\tilde{\sigma}$ ,  $5\tilde{\sigma}$ ,  $1\tilde{\pi}$ ,  $2\tilde{\pi}$ , and  $6\tilde{\sigma}$  valence hole final states. According to the characteristics of XES, these essentially consist of the symmetry resolved atomic p-contributions of the molecular orbitals at the specific core holes.

On this basis we derive a consistent site-specific picture of the surface chemical bond for top and hollow site-bound NO molecules which (for the  $\pi$  channel) is based on the three-center allyl model. For the molecular  $4\tilde{\sigma}$  and  $5\tilde{\sigma}$ -orbitals we also find a significant mixing (rehybridization) according to a three-orbital interaction scheme [18,41], which in particular shows up in the  $4\tilde{\sigma}$  XE signal in the N-edge spectra (in the isolated NO molecule a  $4\sigma$  signal can solely be detected in the O-edge spectra). DF calculations by Staufer et al. [18] have shown that the charge transferred from the adsorbate to the substrate is put into these orbitals, but is not necessarily taken from orbitals of  $\sigma$  symmetry. Generally it should be noted that the XES matrix elements whose square determines the XES intensities depend on the orbital *amplitudes* (which can show phase factors when mixed) and not just on the local *charge density*<sup>1</sup>. For the  $\pi$ -orbitals we find the formation of a totally bonding  $1\tilde{\pi}$  and a ‘lone pair’  $2\tilde{\pi}$  orbital as expected from the allyl model; the third resulting orbital, the unoccupied antibonding  $2\pi^*$ , shows up in NEXAFS. Again, the DF calculations show that the backdonated charge from the substrate to the adsorbate resides in the lower two of these orbitals. Comparison of the XE spectra of hollow site-bound  $v_1$ -NO and on-top-bound  $v_2$ -NO shows two major differences in the  $\sigma$  and the  $\pi$  space. In the  $\sigma$  space the most significant difference is the redistribution of the  $4\sigma$  orbital: while the  $4\tilde{\sigma}$  orbital is localized solely at nitrogen for the  $v_1$ -NO, there is still some  $4\tilde{\sigma}$  density of states at oxygen for  $v_2$ -NO. In  $\pi$  space backdonation from the substrate is more pronounced for the ‘electronegative’  $v_1$ -NO species in comparison to the ‘electropositive’  $v_2$ -NO as indicated by the relative intensities of the ‘lone pair’ emission. These two findings are in line with the weaker intramolecular bond of the  $v_1$ -NO species

in comparison to  $v_2$ -NO which shows up in the elongated NO distance of  $v_1$ -NO and the low vibrational energy [15]. Overall the spectral differences between the two species are not very pronounced. The main difference between pure and O-coadsorbed NO is that for the dense NO rows of the coadsorbed layer a splitting of the  $1\tilde{\pi}$  peak by the broken symmetry is found which does not exist for the less dense, more highly symmetric NO in the pure layer; a difference also exists in the NEXAFS energies for these two types of  $v_1$ -species.

All these conclusions, qualitative ones and those resulting from comparison with the DF calculations [18], are based on the ground state approximation, that is, on the assumption that the orbital structure as seen in XES is that of the ground state, and not that of the core ionized state. This approach is justified by the good agreement between measured spectral shapes and calculated intensity distributions; relative energies agree far less satisfactorily. In view of the expected orbital redistribution by relaxation processes this good agreement is surprising; a theoretical explanation would be highly desirable. Also, the measured differences between XES energies for the same valence hole state reached via different core states, and between these and UPS energies, suggest that the corresponding final states do not necessarily correspond to the same ionic states, but that the different probes reveal differences of relaxation and localization; other reasons for deviations have also been discussed. Nevertheless, the treatment given based on the ground state approximation provides a consistent picture of the surface chemical bond.

### Acknowledgements

The authors sincerely thank Anders Nilsson for clarifying discussions and Alexander Föhlisch for decisive help with the experiments. They are very grateful to Anders Nilsson and Nils Mårtensson for making their excellent endstation available to us for this work, to J. Stöhr and M. Samant for the permission to use their beamline at the ALS Berkeley, and to N. Smith for accepting us at the ALS. This work has been supported financially by

the Deutsche Forschungsgemeinschaft under SFB 338 and Me 266/22, by the Fonds der Chemischen Industrie, and by the Swedish Natural Science Research Council (NFR). The ALS is supported by the Office of Basic Energy Sciences of the US Department of Energy, under Contract No. DE-ACO3-76SF00098.

## References

- [1] A. Nilsson, N. Wassdahl, M. Weinelt, O. Karis, T. Wiell, P. Bennich, J. Hasselström, A. Föhlisch, J. Stöhr, M. Samant, *Appl. Phys. A* 65 (1997) 147.
- [2] A. Nilsson, *J. Electron Spectrosc. Relat. Phenom.* 93 (1998) 143 and references therein.
- [3] N. Wassdahl, A. Nilsson, T. Wiell, H. Tillborg, L.-C. Duda, J.H. Guo, N. Mårtensson, J. Nordgren, J.N. Andersen, R. Nyholm, *Phys. Rev. Lett.* 69 (1992) 812.
- [4] H. Tillborg, A. Nilsson, T. Wiell, N. Wassdahl, N. Mårtensson, J. Nordgren, *Phys. Rev. B* 47 (1993) 16464.
- [5] A. Nilsson, P. Bennich, T. Wiell, N. Wassdahl, N. Mårtensson, J. Nordgren, O. Björneholm, J. Stöhr, *Phys. Rev. B* 51 (1995) 10244.
- [6] A. Nilsson, M. Weinelt, T. Wiell, P. Bennich, O. Karis, N. Wassdahl, A. Nilsson, *Phys. Rev. Lett.* 78 (1997) 147.
- [7] P. Bennich, T. Wiell, O. Karis, M. Weinelt, N. Wassdahl, A. Nilsson, M. Nyberg, L.G.M. Pettersson, J. Stöhr, M. Samant, *Phys. Rev. B* 57 (1998) 9274.
- [8] T. Wiell, J.E. Klepeis, P. Bennich, O. Björneholm, N. Wassdahl, A. Nilsson, *Phys. Rev. B* 58 (1998) 1655.
- [9] M. Weinelt, N. Wassdahl, T. Wiell, O. Karis, J. Hasselström, P. Bennich, A. Nilsson, J. Stöhr, M. Samant, *Phys. Rev. B* 58 (1998) 7351.
- [10] V. Carravetta, L.G.M. Pettersson, O. Vahtras, H. Ågren, *Surf. Sci.* 369 (1996) 146.
- [11] E. Umbach, S. Kulkarni, P. Feulner, D. Menzel, *Surf. Sci.* 88 (1979) 65.
- [12] P. Feulner, S. Kulkarni, E. Umbach, D. Menzel, *Surf. Sci.* 99 (1980) 489.
- [13] K.M. Neyman, N. Rösch, K. Kostov, P. Jakob, D. Menzel, *J. Chem. Phys.* 100 (1994) 2310.
- [14] P. Jakob, M. Stichler, D. Menzel, *Surf. Sci.* 370 (1997) L185.
- [15] M. Stichler, D. Menzel, *Surf. Sci.* 391 (1997) 47.
- [16] M. Stichler, D. Menzel, *Surf. Sci.* 419 (1999) 272.
- [17] M. Stichler, Ph.D. Thesis, TU München 1998.
- [18] M. Staufner, U. Birkenheuer, T. Belling, F. Nörtemann, N. Rösch, M. Stichler, C. Keller, W. Wurth, D. Menzel, L.G.M. Pettersson, A. Föhlisch, A. Nilsson, *J. Chem. Phys.* 111 (1999) 4704.
- [19] T. Wiell, Ph.D. Thesis, Uppsala University, 1995.
- [20] P. Bennich, Ph.D. Thesis, Uppsala University, 1996.
- [21] O. Karis, Ph.D. Thesis, Uppsala University, 1997.
- [22] N. Mårtensson, P. Baltzer, P. Brühwiler, J.O. Forsell, A. Nilsson, A. Stenborg, B. Wannberg, *J. Electron Spec. Relat. Phenom.* 70 (1994) 117.
- [23] J. Stöhr, *NEXAFS Spectroscopy*, Springer Series in Surface Science 25, Springer, New York, 1992.
- [24] E.J. Nordgren, R. Nyholm, *Nucl. Instrum. Meth. Phys. A* 246 (1986) 242.
- [25] E.J. Nordgren, G. Bray, S. Cramm, R. Nyholm, J.-E. Rubensson, N. Wassdahl, *Rev. Sci. Instrum.* 60 (1989) 1690.
- [26] M. Stichler, C. Keller, W. Wurth, S. Lizzit, F. Esch, G. Comelli, D. Menzel (submitted for publication).
- [27] S.H. Payne, H.J. Kreuzer, P. Jakob, D. Menzel, *Surf. Sci.* 424 (1999) 36.
- [28] E.J. McGuire, *Phys. Rev.* 185 (1999); List of fluorescence yields at Geology and Geophysics Department, UC Berkeley, 1998.
- [29] A. Fink, W. Widdra, D. Menzel, unpublished data.
- [30] R. Fink, *J. Chem. Phys.* 106 (1997) 4038.
- [31] P.A. Heimann, P. Jakob, T. Pache, H.-P. Steinrück, D. Menzel, *Surf. Sci.* 210 (1989) 282.
- [32] Resonant inelastic soft X-ray scattering, Proceedings of International Workshop, Walberberg 1996, *Appl. Phys. A* 65 (2) (1997).
- [33] C.T. Chen, R.A. DiDio, W.K. Ford, E.W. Plummer, W. Eberhardt, *Phys. Rev. B* 32 (1985) 8434.
- [34] W. Wurth, C. Schneider, R. Treichler, E. Umbach, D. Menzel, *Phys. Rev. B* 35 (1987) 7741.
- [35] W. Wurth, P. Feulner, D. Menzel, *Phys. Scr. T* 41 (1992) 213.
- [36] A. Sandell, O. Björneholm, A. Nilsson, B. Hernnäs, J.N. Andersen, N. Mårtensson, *Phys. Rev. B* 49 (1994) 10136.
- [37] C. Keller, M. Stichler, G. Comelli, F. Esch, S. Lizzit, W. Wurth, D. Menzel, *Phys. Rev. Lett.* 80 (1998) 1774.
- [38] A. Föhlisch, N. Wassdahl, J. Hasselström, O. Karis, D. Menzel, N. Mårtensson, A. Nilsson, *Phys. Rev. Lett.* 81 (1998) 1730.
- [39] O. Karis, A. Nilsson, M. Weinelt, T. Wiell, C. Puglia, N. Wassdahl, N. Mårtensson, *Phys. Rev. Lett.* 76 (1996) 1380.
- [40] C. Keller, M. Stichler, G. Comelli, F. Esch, D. Menzel, W. Wurth, *Phys. Rev. B* 57 (1998) 11951.
- [41] A. Schichl, N. Rösch, *Surf. Sci.* 137 (1984) 261.
- [42] G. Blyholder, *J. Phys. Chem.* 68 (1964) 2772.
- [43] D.L. DuBois, R. Hoffmann, *Nouv. J. Chim.* 1 (1977) 479.
- [44] T.A. Abright, J.K. Burdett, M.-H. Whangbo, *Orbital Interactions in Chemistry*, Wiley, New York, 1985, p. 36.
- [45] U.v. Barth, G. Grossmann, *Phys. Rev. B* 25 (1982) 5150.
- [46] A. Nilsson, N. Mårtensson, *Physica B* 208/209 (1995) 19.
- [47] L.G.M. Pettersson, H. Ågren, Y. Luo, L. Triguero, *Surf. Sci.* 405 (1998) 1.
- [48] L. Triguero, L.G.M. Pettersson, *J. Phys. Chem. A* 102 (1998) 10599.
- [49] R. van Leeuwen, G.J. Baerends, *Phys. Rev. A* 49 (1994) 2421.
- [50] A. Görling, *Phys. Rev. A* 59 (1999) 3359.